Vis Comput (2018) 34:1677–1689
https://doi.org/10.1007/s00371-017-1441-2

ORIGINAL ARTICLE

Early diagnosis of cirrhosis via automatic location and geometric description of liver capsule

Jingwen Zhao[1] · **Shuo Hong Wang**[1] · **Xiang Liu**[1,2] · **Ye Liu**[3] · **Yan Qiu Chen**[1]

Published online: 19 September 2017

Abstract We propose in this paper an automatic method for early diagnosis of cirrhosis using high-frequency ultrasound images. Instead of analyzing image texture, our method exploits image characteristics of liver capsule. To this end, we first propose a novel spatial context-constrained multi-scale method to accurately extract the boundaries of the liver capsule. Our approach detects all the possible edges in scale space, and the irrelevant edges are then filtered out with a spatial context-based energy function. Secondly on this basis, two novel descriptors are proposed to characterize the geometric properties of liver capsule and the changes of liver capsule with the aggravation of liver cirrhosis. These two descriptors are used as features fed into a support vector machine classifier for quantitative analysis in automatic diagnosis. Experiment results show that the proposed method can reliably localize liver capsule and accurately classify ultrasound liver images into normal and cirrhosis classes automatically.

Keywords Automatic diagnosis · Liver capsule · Spatial context constrained · Scale space · Cirrhosis

1 Introduction

Cirrhosis is a severe liver disease that threatens the life of millions of people [1]. Early diagnosis of cirrhosis [6] is of high value as it enables early treatment that can save life and improve life quality. Currently, many medical imaging techniques [13] have been explored. Compared with other imaging techniques, ultrasound imaging is more preferred [5,7,14] because it is noninvasive, nonradioactive, inexpensive and easy to operate. However, currently the ultrasound images are analyzed by experienced doctors who can be influenced by their subjective differences in knowledge and experience. Differences between individual doctors' subjective diagnosis strongly call for the realization of quantitative diagnosis of cirrhosis in the clinical field [26]. Besides, the number of experienced clinicians carrying vast experience and professional training is not optimistic, especially in underdeveloped areas, which causes heavy burden of diagnoses among doctors. Therefore, researchers with artificial intelligence aspiration strive to develop algorithms for computer-aided early diagnosis of cirrhosis.

Ultrasound images contain various granular structures reflecting the acoustic properties of liver parenchyma [23]. On account of relatively accurate description of these structures via texture features, texture classification is widely used in computer-aided diagnosis [10,11,21,23,24]. However, these methods are semi-automated because various irrelevant signals such as blood vessels and acoustic shadow-

✉ Yan Qiu Chen
chenyq@fudan.edu.cn

Jingwen Zhao
jingwenzhao13@fudan.edu.cn

Shuo Hong Wang
sh_wang@fudan.edu.cn

Xiang Liu
xiangliu09@fudan.edu.cn

Ye Liu
yeliu@njupt.edu.cn

1 School of Computer Science, Shanghai Key Laboratory of Intelligent Information Processing, Fudan University, Shanghai, China

2 School of Electronic and Electric Engineering, Shanghai University of Engineering Science, Shanghai, China

3 College of Automation, Nanjing University of Posts and Telecommunications, Nanjing, China

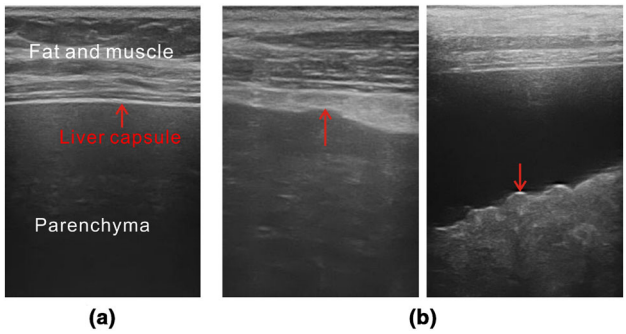

Fig. 1 Normal/cirrhosis liver capsules in ultrasound images

ing scattered in parenchyma demand that regions of interest (ROIs) must be manually selected to avoid noises.

An effective way to overcome the shortcomings is to analyze the changes of liver capsule due to cirrhosis. Ultrasonic echoes from liver capsule, when displayed as an ultrasound image, present normal liver capsule as a fine and smooth curve-like structure on the liver surface [12] (shown in Fig. 1a). As the cirrhosis progresses, the liver capsule is gradually damaged and manifested as unevenly thickened and fractured contours with jagged or wavy changes [3] (shown in Fig. 1b). According to these manifestations, experienced clinicians diagnose cirrhosis and computer-aided diagnosis researchers utilized the observation [2,12,19,22], too. However, no automatic approaches to diagnose cirrhosis are available due to the difficulty in extracting liver capsule and the lack of corresponding features for evaluating the cirrhosis quantitatively.

To overcome these limitations, we propose a method that is able to extract the liver capsule effectively and accurately. Our method consists of two stages. The first stage is a multi-scale edge detector that can locate all curves including capsule and noncapsule structures and noises. These structures are then purified with spatial context constrains in the second stage. We then propose two novel descriptors to describe the geometric characteristics of liver capsule, which are used as features for automatic diagnosis. Finally a support vector machine (SVM) classifier is trained using these two descriptors to classify liver images into normal or cirrhosis class as automatic diagnoses. To support our algorithm, high-frequency ultrasound imaging used in this method greatly improves resolution to help explore the subtle changes of liver capsule, which is conducive to diagnosing cirrhosis automatically. The flowchart of the proposed method is shown in Fig. 2.

The main contributions of this paper are summarized as:

- A novel spatial context-constrained multi-scale method is developed to automatically locate liver capsule.
- Two novel descriptors are proposed for describing the geometric characteristics of liver capsule.

The experiment on 63 liver images shows that this method achieves high accuracy in classifying ultrasound liver images into normal and cirrhosis classes. The credible automatic classification, i.e., automatic diagnosis of cirrhosis, can assist doctors to ease the burden of early diagnosis of cirrhosis, especially in underdeveloped areas where experienced clinicians are not enough.

2 Related work

In order to find an approach to diagnose cirrhosis with the help of computers, many researchers proposed methods based on differences of parenchyma textures to assist clinicians [10,23]. Jitendra et al. [21] applied multi-resolution wavelet packet transform to characterize the texture of parenchyma and trained a genetic algorithm SVM to select features to differentiate abnormal livers from normal ones. Lee et al. [11] proposed to select fractal feature vectors based on M-band wavelet transform and tested various classification algorithms to classify ultrasound liver images. Wu et al. [24] used spatial gray-level co-occurrence matrixes, the Fourier power spectrum, the gray-level difference statistics and the Laws' texture energy measures and applied the Bayes classifier for classification of different types of liver images. However, all these methods extracted features from textures of liver parenchyma that are mixed with blood vessels and acoustic shadowing more or less, which determines that ROIs must be selected manually in general.

Some approaches utilizing liver capsule are also proposed for liver diseases. Dalwadi et al. [2] proposed a method to detect the liver capsule automatically; however, their method lacks quantitative analysis to classify liver images. Liu et al. [12] used progression characteristics of liver capsule and proposed novel features to describe these changes caused by cirrhosis, but their method requires manual selection of

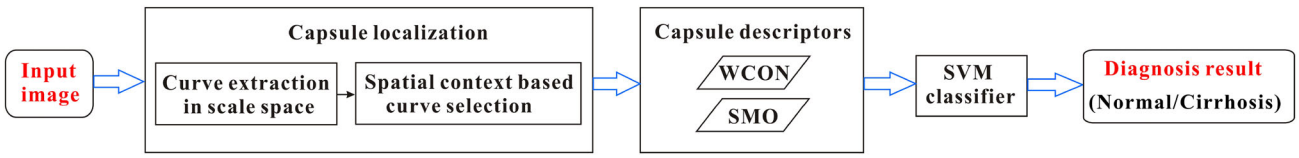

Fig. 2 A flowchart of the proposed automatic diagnosis of cirrhosis

several reference points along the capsule edge for final extraction of liver capsule. Thus, their result is sensitive to the manual selection of initial points. Vicas et al. [19] applied Gabor filters to detect liver capsule automatically; however, what they have done was for quantification of steatosis instead of cirrhosis.

Although lots of line detection methods are proposed, most of them have experienced many unexpected troubles when applied to medical images. On liver images, the capsule line may appear highly fragmented and irregular; moreover, there are similar structures, making it difficult to extract a complete liver capsule and keep the capsule fragmented. The operators [18] such as Sobel, Prewitt, Canny and Snake model, level set [9,25] extract all edges of various tissues, but irrelevant edges cannot be filtered out.

3 Midpoints of bar-shaped lines

Before presenting the proposed method, the identification of midpoints of bar-shaped lines utilized in next sections is firstly introduced.

3.1 Lines in one dimension

Basically, the assumption that lines have the same contrast on both sides is rarely true for real images, including liver images. In fact, curvilinear structures in ultrasound images formed by ultrasonic echoes resembles lines $z(x)$ with a "rounded" profile, such as a parabolic profile. To eliminate noise, lines are convolved with Gaussian kernel as:

$$f(x) = g_\sigma(x) * z(x) \tag{1}$$

In this case, the derivatives of $z(x)$ should be convolved with the derivatives of Gaussian smoothing kernel [4]. Then it is sufficient to determine the midpoints of bar-shaped lines whose derivative $z'(x)$ vanishes.

In principle, a zero crossing detector can be used for this task. But this would yield the position of the line only with pixel accuracy for lines of discrete case. Assuming the discrete image z_n as a piecewise constant function $z(x) = z_n$ for $x \in (n - \frac{1}{2}, n + \frac{1}{2}]$, the second Taylor polynomial of z_n is examined instead of zero crossing [16]. Let r, r' and r'' be the locally estimated derivatives at point n of the image after convolution with corresponding Gaussian kernel. Then the Taylor polynomial is given by

$$p(x) = r + r'x + \frac{1}{2}r''x^2 \tag{2}$$

The midpoints of the line, i.e., the point where $p'(x) = 0$ is

$$x = -\frac{r'}{r''} \tag{3}$$

Falling within the pixel's boundaries, i.e., $x \in [-\frac{1}{2}, \frac{1}{2}]$ is required, in order for the point n to be declared a midpoint of the line.

The detailed mathematical proof is in [16,17].

3.2 Lines in two dimensions

Lines in two dimensions (2D) can be modeled as curves $s(t)$ in image $z(x, y)$. Assume the direction perpendicular to the line $s'(t)$ as $n(t)$; then, the first directional derivative in the direction $n(t)$ will vanish. This direction can be obtained by Hessian matrix

$$\mathcal{H}(x, y) = \begin{pmatrix} r_{xx} & r_{xy} \\ r_{xy} & r_{yy} \end{pmatrix} \tag{4}$$

since its eigenvector corresponding to the eigenvalue of minimum absolute value is the direction of the line, i.e., $s'(t)$.

Let the direction perpendicular to $s'(t)$ be given by (n_x, n_y) subjected to $||(n_x, n_y)||_2 = 1$. As in the 1D case, a quadratic polynomial is used to determine whether the first directional derivative along (n_x, n_y) vanishes within the current pixel. The Taylor polynomial in 2D is:

$$p(x, y) = r + r_x x + r_y y + \frac{1}{2}r_{xx}x^2 + r_{xy}xy + \frac{1}{2}r_{yy}y^2 \tag{5}$$

where the partial derivatives r_x, r_y, r_{xx}, r_{xy} and r_{yy} of the image are estimated by convolving the image $z(x, y)$ with 2D Gaussian partial derivative kernels.

Assume (p_x, p_y) as the midpoints of the line, it satisfies

$$\begin{cases} (p_x, p_y) = (tn_x, tn_y), \\ p'(p_x, p_y) = 0 \end{cases} \tag{6}$$

thus,

$$t = -\frac{r_x n_x + r_y n_y}{r_{xx}n_x^2 + 2r_{xy}n_x n_y + r_{yy}n_y^2} \tag{7}$$

Again, point (p_x, p_y) could be determined as a midpoint of the line only if $(p_x, p_y) \in [-\frac{1}{2}, \frac{1}{2}] \times [-\frac{1}{2}, \frac{1}{2}]$.

After the midpoints are identified, lines are obtained since those extracted line pixels are not individual but originally linked as lines.

4 Liver capsule localization

Localizing the liver capsule is a challenging task. The capsule line may appear highly fragmented and irregular; moreover,

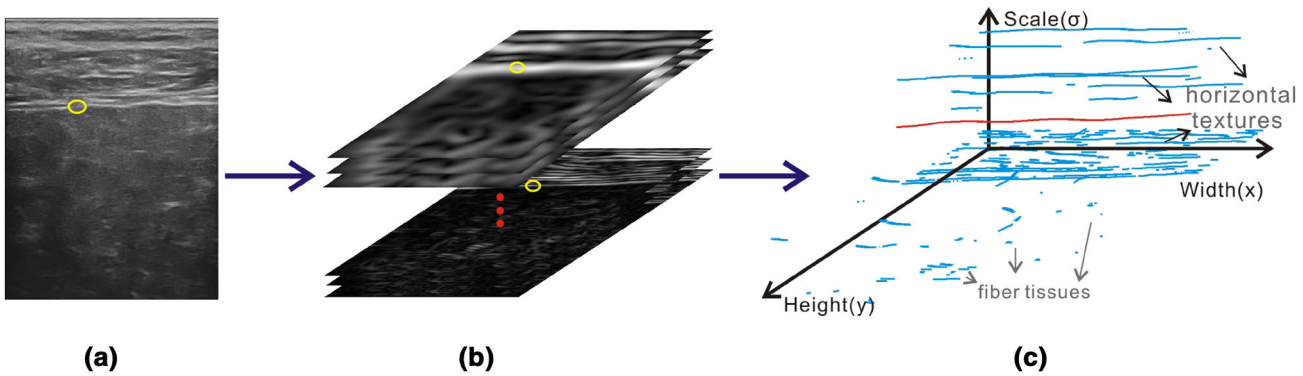

Fig. 3 Localizing the liver capsule. **a** Original image I_0. **b** Ω: gradient image sequences $e(x, y, \sigma)$ in scale space of I_0. **c** The optimum curve colored red among all detected edges. Disconnected part circled yellow in I_0 reappears in gradient images in Ω

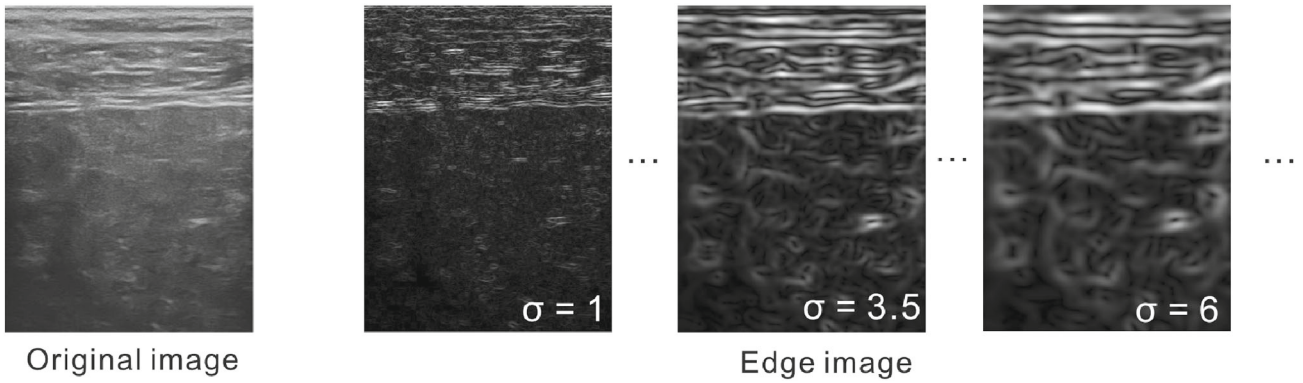

Fig. 4 In the original image, fragmented liver capsule segments are mixed with similar structures. As σ increases, edges of liver capsule are gradually clear and linked into a continuous line

there are similar structures on the image, making it difficult to extract a complete liver capsule. We propose in this paper a method that is able to extract the liver capsule effectively and accurately. Our approach firstly detects all the possible edges in scale space, and the irrelevant edges are then filtered out with a spatial context-based energy function.

4.1 Curve extraction in scale space

Let $z(x, y)$ indicate image I_0, and let Ω be a bounded subset of R^3 indicating gradient image sequences $e(x, y, \sigma)$ in scale space of I_0 as shown in Fig. 3:

$$e(x, y, \sigma) = \sqrt{f_x(x, y, \sigma)^2 + f_y(x, y, \sigma)^2} \tag{8}$$

where

$$f(x, y, \sigma) = g(x, y, \sigma) * z(x, y) \tag{9}$$

$$g(x, y, \sigma) = \frac{1}{2\pi\sigma^2} e^{-\frac{x^2+y^2}{2\sigma^2}} \tag{10}$$

In the image of the absolute value of the gradient of I_0^σ, the desired edges appear as bright lines. The edges are gradually clear as σ increases and an uncertain but relatively larger σ will integrate boundaries of broken liver capsule into a continuous line (see Fig. 4).

These edges in Ω are extracted via methods in Sect. 3. Each point at different scale is defined as (p_x^σ, p_y^σ) and it will be declared as a midpoint of edges if $(p_x^\sigma, p_y^\sigma) \in [-\varepsilon_p, \varepsilon_p] \times [-\varepsilon_p, \varepsilon_p]$. Here we replace $\frac{1}{2}$ with ε_p which is slightly larger than $\frac{1}{2}$ to ensure midpoints can be linked as curves. Afterward curves of various scales are extracted, which includes liver capsule, fiber tissues in liver parenchyma and horizontal textures of the upper layer.

4.2 Spatial context-based curve selection

After excessive amount of curve structures has been extracted, false ones must be filtered out.

Assume all curves with the total number of $\eta(\mathfrak{B})$ in scale space are contained in set $\mathfrak{B} = \{\mathcal{B}_i | i \in [1, \eta(\mathfrak{B})]\}$ where $\mathcal{B}_i = \{V_j | j \in [1, \lambda(\mathcal{B}_i)]\}$ as shown in Fig. 5. Here $\lambda(\mathcal{B}_i)$ denotes the length of $\mathcal{B}_i$ and $V_j = V(x_j, y_j, \sigma)$ indicates a point on the curve detected from image at scale σ. Points in

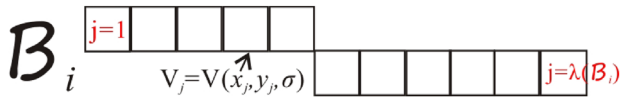

Fig. 5 An illustration of $\mathcal{B}_i$ that is one curve among $\mathfrak{B}$, i.e., $\mathcal{B}_i \in \mathfrak{B}$

one curve have the same scale σ. In this paper, $\eta(.)$ denotes the number of curves in a set and $\lambda(.)$ is the length of a curve.

In high-frequency ultrasound images of liver superficial sections, the desired curves, i.e., the capsule boundaries that partition brighter capsule and darker parenchyma, basically meet three conditions as shown in Fig. 3c:

Shorter distance Horizontal textures in fat and muscle layer are similar with liver capsule in length, but they are all in upper layer that is above the capsule, i.e., further from the image bottom.

Longer length Vertical up from the bottom of liver image, the lower parenchyma layer is usually scattered with fiber tissues formed around nodules in small size.

Smaller scale A curve at a relatively small scale is more similar with liver capsule in changes of curvature.

These three requirements are determined by the clinical ultrasound that liver tissue is scanned under xiphoid and between the right rib. Among these three factors, fiber tissues are much shorter than liver capsule in length while horizontal textures are very close to liver capsule in distance, which calls for a larger parameter for the distance. In addition, the parameter for scale is smaller since a small scale just closes the gap between shapes and does not influence the location. Thus, this paper establishes a spatial context-based energy function taking distance, length and scale into consideration with different parameters weighing the strength of each constraint:

$$E_{\text{edge}}(\mathcal{B}_i) = \alpha E_{\text{distance}} + E_{\text{length}} + \beta E_{\text{scale}} \tag{11}$$

where

$$E_{\text{distance}} = \exp\left(\frac{1}{H \cdot \lambda(\mathcal{B}_i)} \sum_{k=1}^{\lambda(\mathcal{B}_i)} y_k - 1\right) \tag{12}$$

$$E_{\text{length}} = \exp\left(-\frac{1}{W} \max_{u,v \in [1,\lambda(\mathcal{B}_i)]} (x_u - x_v)\right) \tag{13}$$

$$E_{\text{scale}} = \exp\left(\frac{\sigma}{\varepsilon_{e-\text{scale}}} - 1\right) \tag{14}$$

The width and height of image I_0 are denoted as W and H. The maximum scale $\varepsilon_{\text{e-scale}}$ when extracting curves is limited to 20 to avoid consuming too much time during solving the energy function. Function exp is adopted to normalize each constraint in range [0, 1].

The optimum curve (capsule edge) $\mathcal{B}_{\text{opt}}$ is selected by considering the minimization problem:

$$\inf_{\mathcal{B}_i \in \mathfrak{B}} (E_{\text{edge}}(\mathcal{B}_i)) \tag{15}$$

An illustration is shown in Fig. 6

5 Description of the liver capsule

In order to describe geometric characteristics of liver capsule and changes in cirrhosis progression, two novel descriptors are proposed for quantitative analysis in automatic diagnosis. One descriptor SMO is for smoothness and the other one WCON is for width-based continuity. Samples of automatic extraction of liver capsule, including an continuous capsule edge and original fragmented capsule segments in each image, are illustrated in Fig. 9.

5.1 Smoothness

The inspiration of SMO comes from more jagged and wavier contours of liver capsule which leads to constantly changing slopes during the cirrhosis progression.

Assume the optimum capsule edge $\mathcal{B}_{\text{opt}}$ is composed of a point set with n_b points contained: $\mathcal{P}^b = \{p_1^b, \ldots, p_{n_b}^b\}$. Denote the curve slopes every ε_k point as $\mathcal{K} = \{k_1, \ldots, k_{n_k}\}$ in point set $\mathcal{P}^b$. Then the smoothness of the capsule is obtained as:

$$\text{SMO} = \frac{1}{n_k^2} \sum_{i=1}^{n_k} \sum_{j>i}^{n_k} (k_i - k_j)^2 \tag{16}$$

Here ε_k is assigned five to diminish too large slopes between adjacent pixels in a line.

5.2 Width-based continuity

Generally, liver capsule becomes increasingly unevenly thickened and discontinuous as cirrhosis progresses; moreover, liver ascites sometimes appear, which motivates us to describe cirrhosis via width-based continuity. However, the original continuity of each liver capsule is in lack considering that the obtained boundaries of liver capsule are connected as a continuous line via σ in Sect. 4.1.

For original fragmented segments of liver capsule, a width-adaptive extraction method is employed.

Liver capsule seems discontinuous and brighter line of uncertain width in high-frequency ultrasound images; thus, its midline can be detected by the method of midpoints identification discussed in Sect. 3. However, with the aggravation of liver cirrhosis, the width of liver capsule increases

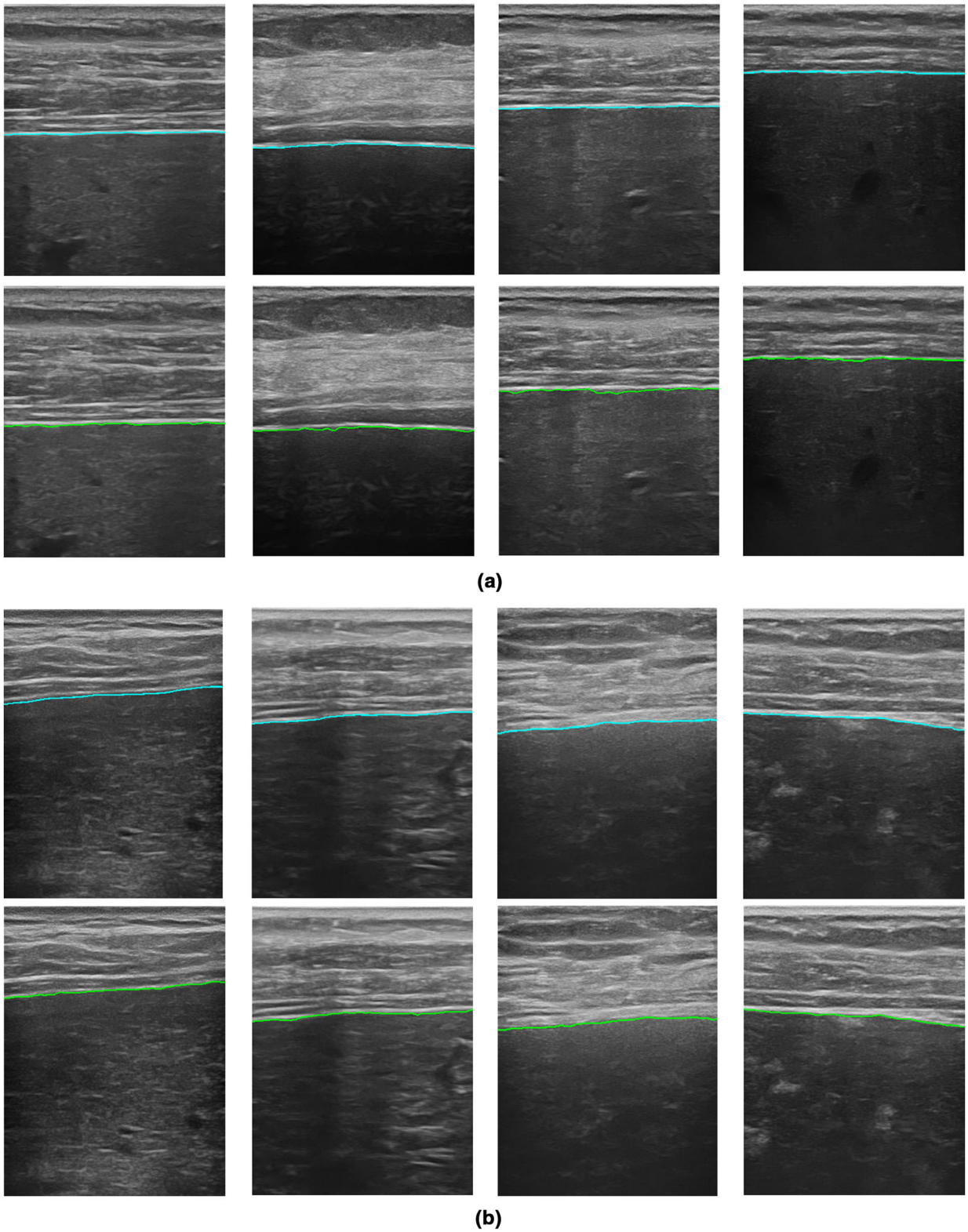

Fig. 6 Automatic localization of liver capsule (row one in blue) and corresponding manually labeled liver capsule (row two in green) in each subfigure. As cirrhosis condition becomes worse from (**a**) to (**d**) (normal, mild, moderate, severe), liver capsule lost its original smooth and fine characteristic, and becomes thicken, jagged or wavy. The discontinuity is also invisible during the localization while fractured liver capsule is visible in Fig. 9

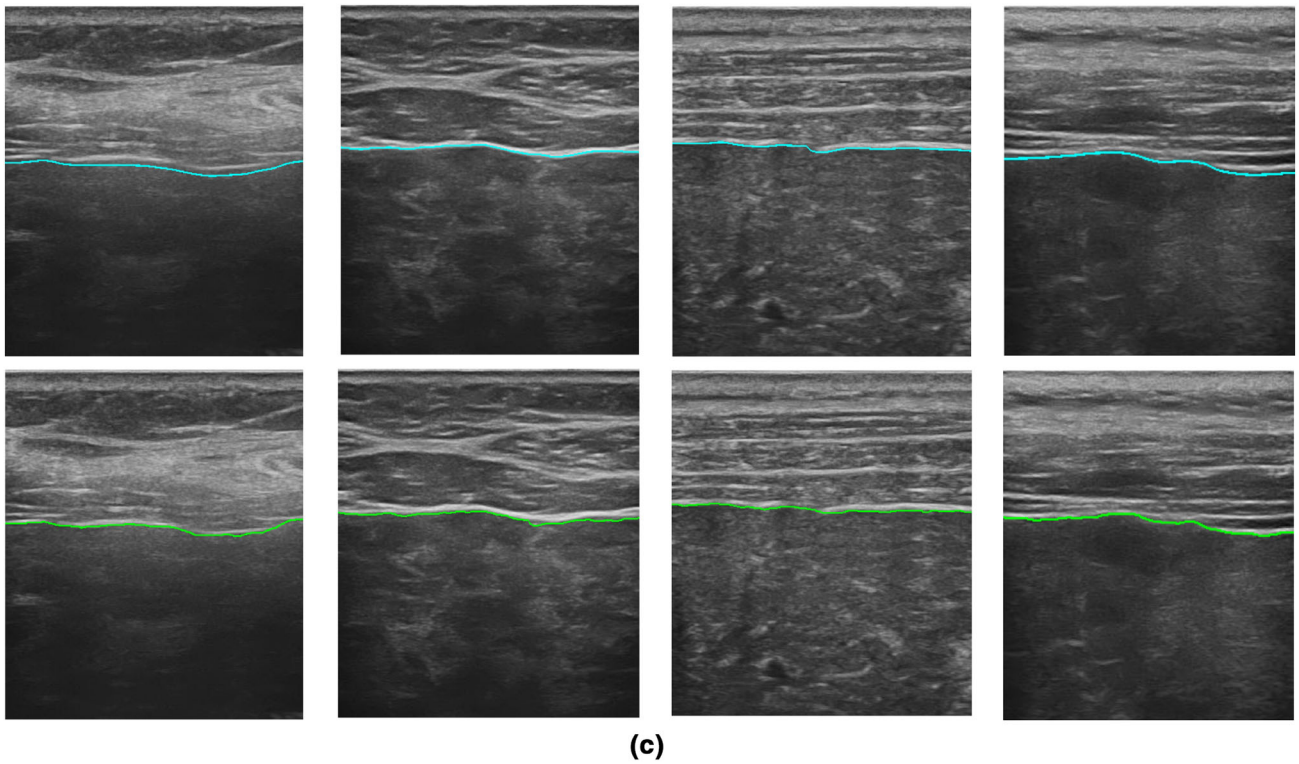

(c)

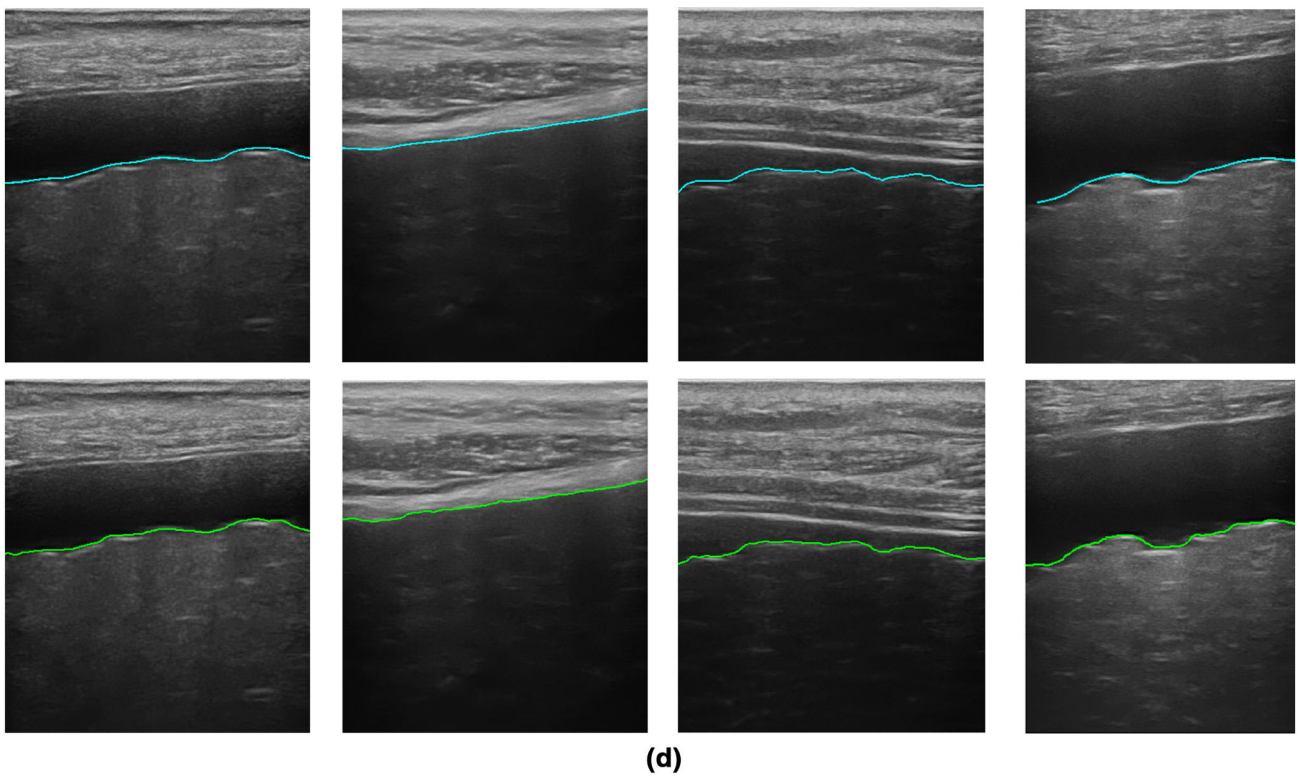

(d)

Fig. 6 continued

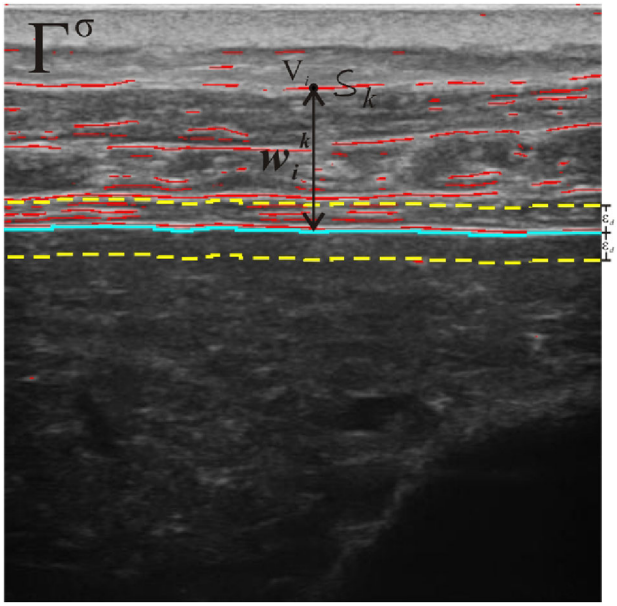

Fig. 7 Identify liver capsule line inside the range around the optimum capsule colored blue from the potential curve segments colored red at $\sigma = 3.5$. Its result is shown in Fig. 8

in high-frequency images, which results in the failure of bar-shaped line extraction based on fixed width. To solve this problem, we utilize the identification that σ in Gaussian kernel for noise reduction is associated with the width of liver capsule as [17] and the experiments have proved. The max half width of liver capsule in ultrasound image is limited to $\varepsilon_w = 20$. Midpoints of bar-shaped lines are identified in image I_0 at different σ in scale space. These midpoints at each σ are shaped as lines in varied length scattered around the image as Fig. 7 illustrates. The detected lines are assumed as candidate capsule curve segments written as $\Gamma^\sigma = \{\mathcal{S}_i | i = [1, \eta(\Gamma^\sigma)]\}$. Each segment consists of $\lambda(\mathcal{S}_i)$ discrete points: $\mathcal{S}_i = \{V_j | j = [1, \lambda(\mathcal{S}_i)]\}$ and $V_j = V(x_j, y_j, \sigma)$. We selected the final capsule curve segments from Γ^σ based on an obvious observation 1) the distance between true midlines and edge is similar: 2) the distance between true midlines and edge is small 3) the ratio between length of true midlines and length of the edge is large in one liver image. The set of resultant segments is written as $\mathcal{L}^\sigma = \{S_i | i \in [1, \eta(\mathcal{L}^\sigma)]\}$ where $\eta(\mathcal{L}^\sigma)$ indicates the number of curve segments $\mathcal{S}_i$ and obtained by solving the multi-objective optimization problem:

$$\arg\max_{\Gamma^\sigma} \left[\frac{1}{n_w^2} \sum_{k=1}^{\eta(\Gamma^\sigma)} \sum_{i=1}^{n_w} \sum_{j>i}^{n_w} (w_i^k - w_j^k)^2 \delta(\mathcal{S}_k), \right.$$
$$\left. \frac{1}{n_w} \sum_{k=1}^{\eta(\Gamma^\sigma)} \sum_{i=1}^{n_w} w_i^k \delta(\mathcal{S}_k), \right.$$
$$\left. \frac{1}{\lambda(\mathcal{B}_{\text{opt}})} \sum_{k=1}^{\eta(\Gamma^\sigma)} \delta(\mathcal{S}_i)\lambda(\mathcal{S}_i) \right]$$
$$\text{s.t.} \begin{cases} w_i^k = y_i^{\mathcal{B}_{\text{opt}}} - y_i^{\mathcal{S}_k}, \\ n_w = \sum_{k=1}^{\eta(\Gamma^\sigma)} \lambda(\mathcal{S}_k) \\ \bigcap(X_i, X_j) = \emptyset \\ \delta(x) = \begin{cases} 0, & if x \notin \mathcal{L}^\sigma \\ 1, & else \end{cases} \end{cases} \tag{17}$$

where X_i is the x coordinate set of capsule curve segment $\mathcal{S}_i$ and $y_i^{\mathcal{S}_k}$ is the y coordinate of point V_i in the curve segment $\mathcal{S}_k$. As defined in Sect. 4.2, $\lambda(.)$ is the length of a curve and η denotes how many curves a set contains. We narrow the search of the optimization problem since the liver capsule does not appear ε_d pixels away from the optimum capsule edge $\mathcal{B}_{\text{opt}}$ as Fig. 7 illustrates in yellow color. ε_d is assigned as 30 in consideration that it is bigger than the half maximum width ε_w of liver capsule and dramatically cuts down search space.

Those detected lines at each σ, i.e., potential liver capsule lines are denoted as $\mathfrak{L} = \{\mathcal{L}^\sigma | \sigma \in [1, \varepsilon_{w-\text{scale}}]\}$ where $\mathcal{L}^\sigma = \{V_j | j \in [1, \lambda(\mathcal{L}^\sigma)]\}$, $\lambda(\mathcal{L}^\sigma)$ is the length of $\mathcal{L}^\sigma$ as Fig. 5 shows. The line that satisfies the criterion which measures the completeness of those plausible liver capsule lines is declared the optimum detection of liver capsule $\mathcal{D}_{\text{opt}} = \mathcal{L}^i$ (Fig. 8). The criterion is defined as

$$i = \arg\max_{\sigma \in [1, \varepsilon_{w-\text{scale}}]} \frac{\lambda(\mathcal{L}^\sigma)}{\lambda(\mathcal{B}_{\text{opt}})} \tag{18}$$

Assume the obtained liver capsule $\mathcal{D}_{\text{opt}}$ is composed of a point set $\mathcal{P}^d = \{p_1^d, \ldots, p_{n_d}^d\}$ consisting of n_d points where $p_1^d = (x_1^d, y_1^d, \sigma)$. The number of boundary points n_b has been introduced in Sect. 5.1.

Then WCON is defined as:

$$\text{WCON} = \frac{\text{con}}{\text{width}} \tag{19}$$

where

$$\text{con} = \frac{n_d}{n_b} \tag{20}$$

$$\text{width} = \frac{\sum_{i=1}^{n_d} (y_i^b - y_i^d)}{n_d} \tag{21}$$

5.3 Classification via learning

Now that we have constructed features that contain discrimination information to tell whether a liver image is normal, we need a classifier that can learn from annotated images to classify the new images.

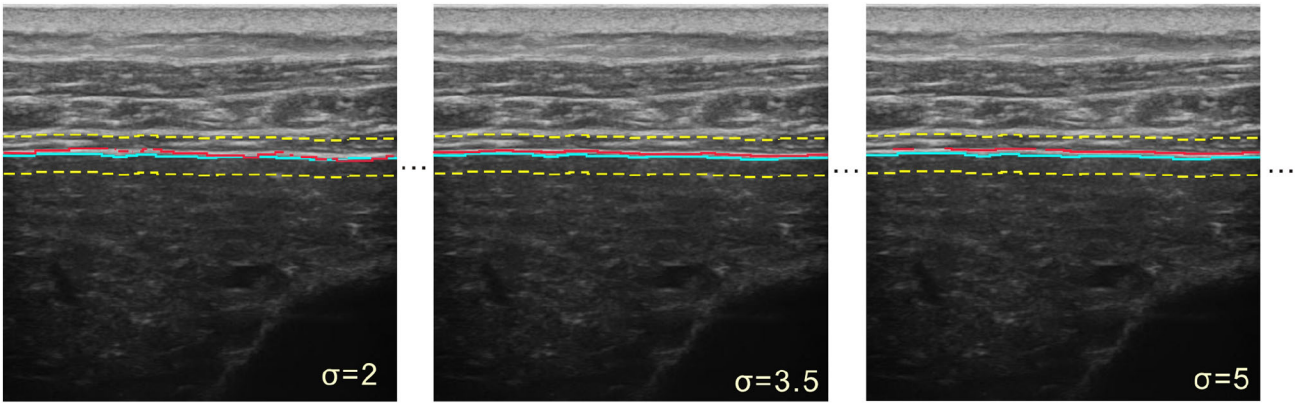

Fig. 8 After the optimum capsule edge is localized, the fragmented midline of capsule is detected at each σ within a small range $\varepsilon_{w-\text{scale}}$. The above three pictures illustrate the extracted liver capsule line at $\sigma = 2, 3.5, 5$. Usually if the total length of the capsule segments is larger, we think it detect a more precious capsule at a better σ. For the capsule above, 3.5 is the optimum σ

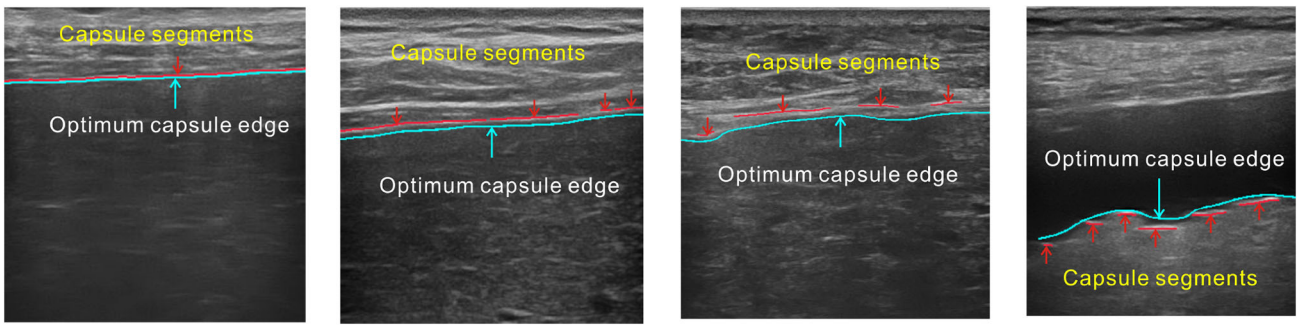

Fig. 9 Samples of automatic extraction of liver capsule: Changes of liver capsule as cirrhosis condition becomes worse from left (normal) to right (severe)

In this paper, a support vector machine (SVM) classifier is used to obtain accurate classification of normal and cirrhosis images. SVM has shown good performance in nonlinear classification problems when facing small training set and high dimension [15]. Before using SVM, the extracted features are first normalized to [0, 1] to avoid bias caused by unbalanced feature values. Then one-vs-rest strategy is employed to classify the samples into 4 classes. The accuracy test is performed using a K-fold cross-validation strategy where $K = 5$. Evaluation is accomplished for the average performance of each method by performing the classification for 50 times.

Samples of automatic extraction of liver capsule are illustrate in Fig. 9.

6 Experiments

We performed experiments on a dataset acquired from hospital and compared the proposed method with three state-of-the-art approaches.

6.1 Data collection

The superficial section images of the liver were obtained using a Voluson E8 ultrasound machine with a high-frequency probe. Liver tissue was scanned under xiphoid and between the right rib by the ultrasound whose frequency is 4-10 MHz. Normal subjects and cirrhosis sufferers were randomly selected under the premise of no significant differences in age, gender and weight. The progression of cirrhosis is divided into 3 stages according to Child–Pugh standard: mild, moderate and severe. The diagnosis of cirrhosis was confirmed by laboratory examination, ultrasound and CT. In this paper, cases complicated with fatty liver, schistosome hepatic disease and other organic liver diseases were excluded.

Due to the size of the patient's body and the thickness of the fat layer, it is necessary to obtain a high-resolution image by adjusting the distance and frequency of the ultrasonic probe. The height of obtained images is 262 ± 36 and the width is 375 ± 29.

Table 1 Accuracy of capsule localization

Groups	Case number	Accuracy (%)
Normal	20	100
Mild	16	98.75
Moderate	16	93.75
Severe	11	83.63

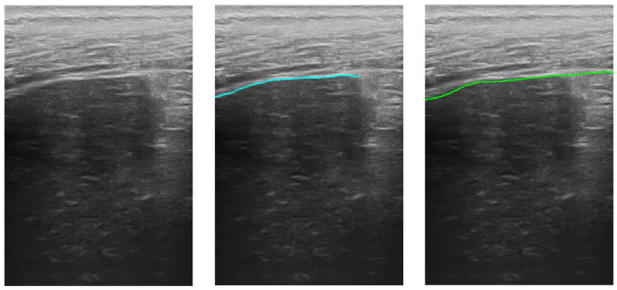

Fig. 10 False detection. **a** Original image, **b** localization, **c** ground truth

6.2 Evaluation and discussion

6.2.1 Results of capsule localization

Liver capsule is localized automatically via a spatial context-based curve selection method. To evaluate the performance, ground truth capsule is labeled manually and the results of localization are considered to be correct if Euclidean distance between detected capsule edge and ground truth capsule is less than a threshold (we chose 10). The proposed method achieved higher accuracy on normal liver images due to stronger intensity contrast and better continuity of liver capsule. The statistic results are presented in Table 1, and Fig. 6 shows the localization results of liver capsule and corresponding ground truth, respectively, in four stages. The proposed method achieved higher accuracy on normal liver images than others, as the capsules in images of normal livers are clearer and smoother.

On some images, the edges of liver capsule appear to be obscured by imaging noise, which seriously affects our edge-based localization as Fig. 10 shows.

6.2.2 Difference analysis of descriptors

The performance evaluation of the proposed descriptors is carried out using two different metrics. In medical field, difference analysis is the traditional metric to estimate the significance of features, while researchers in computer science adopt the accuracy of classifying samples into correct classes.

Table 2 Difference analysis inside each group

Groups	SMO	WCON
Normal	4.26 ± 1.05	5.11 ± 1.99
Mild	6.37 ± 2.54	2.32 ± 1.63
Moderate	13.96 ± 7.03	1.24 ± 0.66
Severe	22.39 ± 11.99	0.19 ± 0.53

Table 3 Pairwise difference analysis

Groups	Levels	SMO	WCON
Normal	Mild	0.033	0.000
	Moderate	0.000	0.000
	Severe	0.010	0.000
Mild	Normal	0.033	0.000
	Moderate	0.005	0.125
	Severe	0.020	0.000
Moderate	Normal	0.000	0.000
	Mild	0.005	0.125
	Severe	0.320	0.000
Severe	Normal	0.010	0.000
	Mild	0.020	0.000
	Moderate	0.320	0.000

For difference analysis, ANOVA was used inside each group for mean $\pm$ standard deviation, and Dunnett T3 test was employed for pairwise comparison between two groups. Statistical differences were considered significant at $P < 0.05$. Previous computer-aided methods failed to carry on difference analysis because they used combined features in high dimension for classification, but each dimension is actually meaningless to clinical features of liver images.

Cirrhosis results in smaller WCON as discontinuity decreases capsule length and thickness grows, and SMO is larger since more jagged and wavier contours of liver capsule lead to constantly changing slopes during cirrhosis. Table 2 shows quantitative analysis of these changes happened to liver capsule during cirrhosis in the form of two features.

The differences between normal and cirrhosis images are statistically significant ($P < 0.05$) for WCON and SMO in Table 3, which proves the proposed features can differentiate normal and cirrhosis cases significantly even if this case is in an early level (mild). However, the differences between three cirrhosis levels are poor, especially between mild and moderate levels ($P = 0.125$), and moderate and severe levels ($P = 0.320$).

Accuracy is also tested to classify normal cases and is discussed when compared with other approaches.

Table 4 Accuracy comparison of four methods

Methods	Normal (%)	Cirrhosis		
		Mild (%)	Moderate (%)	Severe (%)
The proposed	**92.50**	**74.71**	70.08	**86.17**
Kalyan et al. [8]	90.12	74.30	**75.03**	80.06
Lee et al. [11]	70.06	68.31	70.19	73.33
Virmani et al. [20]	70.77	68.90	73.52	78.81

Table 5 Fscore comparison of four methods

Methods	Normal (%)	Cirrhosis		
		Mild (%)	Moderate (%)	Severe (%)
The proposed	**91.36**	**72.45**	69.83	**81.14**
Kalyan et al. [8]	86.12	65.75	68.42	71.13
Lee et al. [11]	68.15	67.80	67.43	70.66
Virmani et al. [20]	71.29	66.67	**70.40**	74.46

6.2.3 Comparisons and discussions

Several related works have been proposed to diagnose cirrhosis by manually extracting ROIs and analyzing textures of parenchyma in low-frequency ultrasound images. Three representative approaches are applied in the dataset of high-frequency images in this section. Kalyan [8] applied gray-level run length matrix (GLRLM) to analyze parenchyma textures. Lee et al. [11] obtained fractal dimension sequences on images after wavelet transformation and [20] claimed Gabor filters were extremely useful for providing multi-scale texture description. An accuracy contrast and an fscore comparison are shown in Tables 4 and 5 where our method is expressed as "Prop," and best results are labeled in bold.

Comparison results show that the proposed method using clinical features of liver capsule achieved better performance when differentiating normal and cirrhosis livers. The proposed method achieves the highest accuracy and fscore when classifying normal and cirrhosis liver images. Different from the proposed method that utilizes changes of liver capsule, the compared approaches extract features from textures of liver parenchyma. However, liver parenchyma textures are mixed with blood vessels and acoustic shadowing, which leads to worse accuracy and ineluctable manually selection of ROIs. Meanwhile, features extracted from textures are meaningless in clinical manifestation. Conversely, benefited from the proposed spatial context-based curve selection approach, automatic diagnosis realizes here. Moreover, the proposed descriptors are corresponding to the characteristic changes of liver capsule during the progression of cirrhosis.

Classifying cirrhosis into three levels is also evaluated. Although other methods achieve higher or similar accuracy in some levels, the higher accuracies obtained by these methods are not convincing enough (<0.8). Therefore, the proposed method is more effective than other methods on early diagnosis of cirrhosis since it finishes the classification automatically and achieves a high and convincing accuracy in classifying normal liver images.

Table 6 Test with one feature

Groups	Features	Accuracy (%)	Fscore (%)
Normal	SMO	80.38	77.58
	WCON	88.50	83.41
Mild	SMO	72.22	68.02
	WCON	70.80	67.40
Moderate	SMO	77.92	71.79
	WCON	70.51	68.35
Severe	SMO	85.17	76.73
	WCON	88.10	88.39

To estimate the effectiveness of each feature in the proposed method when identifying normal liver images, classification accuracy and fscore using only one feature is obtained in Table 6. Comparison results show that the feature WCON exceeds SMO in classification accuracy of three groups, which is consistent with difference analysis of the proposed method in Table 3.

7 Conclusion

We have proposed an automatic method for early diagnosis of cirrhosis using high-frequency ultrasound images. Instead of analyzing image texture, our method exploits image characteristics of liver capsule. To this end, we first propose a novel spatial context-constrained multi-scale method to accurately extract the boundaries of the liver capsule. Our approach detects all the possible edges in scale space, and the irrelevant edges are then filtered out with a spatial context-based

energy function. Secondly on this basis, two novel descriptors are proposed to characterize the geometric properties of liver capsule and the changes of liver capsule with the aggravation of liver cirrhosis. These two descriptors are used as features fed into a support vector machine (SVM) classifier for quantitative analysis in automatic diagnosis. Experiment results show that the proposed method can reliably localize liver capsule and accurately classify ultrasound liver images into normal and cirrhosis classes automatically.

Since a certain estimation of tortuosity measures lines with a constant curvature and relative change of curvature, we suppose it could potentially serve as another feature to describe smoothness of liver capsule. Furthermore, comparisons with other methods demonstrate that changes of parenchyma textures are also potential feature. As long as we overcome the limitations that blood vessels and acoustic shadowing serve as noises in parenchyma, ROIs of parenchyma can be cropped automatically and features are easily obtained. We will focus on them in the feature work.

Acknowledgements This work is supported by Science and Technology Commission of Shanghai Municipality, Grant No. 17ZR1402300. National Natural Science Foundation of China (Grant No. 61602255). Natural Science Foundation of the Jiangsu Higher Education Institutions of China (Grant No.16KJB520032).

References

1. Abubakar, I., Tillmann, T., Banerjee, A.: Global, regional, and national age-sex specific all-cause and cause-specific mortality for 240 causes of death, 1990–2013: a systematic analysis for the global burden of disease study 2013. Lancet **385**(9963), 117–171 (2015)
2. Dalwadi, M.N., Khandhar, D., Wandra, K.H.: Automatic boundary detection and generation of region of interest for focal liver lesion ultrasound image using texture analysis. IJARCET **2**, 2369–2373 (2013)
3. Di Lelio, A., Cestari, C., Lomazzi, A., Beretta, L.: Cirrhosis: diagnosis with sonographic study of the liver surface. Radiology **172**(2), 389–392 (1989)
4. Florack, L.M., ter Haar Romeny, B.M., Koenderink, J.J., Viergever, M.A.: Scale and the differential structure of images. Image Vis. Comput. **10**(6), 376–388 (1992)
5. Gaiani, S., Gramantieri, L., Venturoli, N., Piscaglia, F., Siringo, S., D'errico, A., Zironi, G., Grigioni, W.: What is the criterion for differentiating chronic hepatitis from compensated cirrhosis? A prospective study comparing ultrasonography and percutaneous liver biopsy. J. Hepatol. **27**(6), 979–985 (1997)
6. Iloeje, U.H., Yang, H.I., Su, J., Jen, C.L., You, S.L., Chen, C.J., et al.: Predicting cirrhosis risk based on the level of circulating hepatitis b viral load. Gastroenterology **130**(3), 678–686 (2006)
7. Kadah, Y.M., Farag, A.A., Zurada, J.M., Badawi, A.M., Youssef, A.B.: Classification algorithms for quantitative tissue characterization of diffuse liver disease from ultrasound images. IEEE Trans. Med. Imaging **15**(4), 466–478 (1996)
8. Kalyan, K., Jakhia, B., Lele, R.D., Joshi, M., Chowdhary, A.: Artificial neural network application in the diagnosis of disease conditions with liver ultrasound images. Adv. Bioinform. **2014**, Article ID 708279 (2014). doi:10.1155/2014/708279
9. Kass, M., Witkin, A., Terzopoulos, D.: Snakes: active contour models. Int. J. Comput. Vis. **1**(4), 321–331 (1988)
10. Lee, W.L.: An ensemble-based data fusion approach for characterizing ultrasonic liver tissue. Appl. Soft Comput. **13**(8), 3683–3692 (2013)
11. Lee, W.L., Chen, Y.C., Hsieh, K.S.: Ultrasonic liver tissues classification by fractal feature vector based on m-band wavelet transform. IEEE Trans. Med. Imaging **22**(3), 382–392 (2003)
12. Liu, X., Song, J.L., Zhao, J.W., Chen, Y.Q., Zhang, J.Q.: Extracting and describing liver capsule contour in high-frequency ultrasound image for early HBV cirrhosis diagnosis. In: IEEE International Conference on Multimedia and Expo (ICME), pp. 1–6. IEEE (2016)
13. McPhee, S.J., Papadakis, M.A., Tierney, L.M.: Current medical diagnosis & treatment. McGraw-Hill Medical, New York (2010)
14. Raeth, U., Schlaps, D., Limberg, B., Zuna, I., Lorenz, A., Van Kaick, G., Lorenz, W.J., Kommerell, B.: Diagnostic accuracy of computerized b-scan texture analysis and conventional ultrasonography in diffuse parenchymal and malignant liver disease. J. Clin. Ultrasound **13**(2), 87–99 (1985)
15. Smola, A.J., Schölkopf, B.: A tutorial on support vector regression. Stat. Comput. **14**(3), 199–222 (2004)
16. Steger, C.: Extracting curvilinear structures: a differential geometric approach. In: Computer Vision ECCV'96, pp. 630–641 (1996)
17. Steger, C.: An unbiased detector of curvilinear structures. IEEE Trans. Pattern Anal. Mach. Intell. **20**(2), 113–125 (1998)
18. Torre, V., Poggio, T.A.: On edge detection. IEEE Trans. Pattern Anal. Mach. Intell. **2**, 147–163 (1986)
19. Vicas, C., Nedevschi, S., Lupsor, M., Badea, R.: Automatic detection of liver capsule using Gabor filters. Applications in steatosis quantification. In: IEEE 5th International Conference on Intelligent Computer Communication and Processing. ICCP 2009, pp. 133–140. IEEE (2009)
20. Virmani, J., Kumar, V., Kalra, N., Khandelwal, N.: Prediction of liver cirrhosis based on multiresolution texture descriptors from b-mode ultrasound. Int. J. Converg. Comput. **1**(1), 19–37 (2013)
21. Virmani, J., Kumar, V., Kalra, N., Khandelwal, N.: SVM-based characterization of liver ultrasound images using wavelet packet texture descriptors. J. Digital Imaging **26**(3), 530–543 (2013)
22. Wang, S.H., Liu, X., Zhao, J., Song, J.L., Zhang, J.Q., Chen, Y.Q.: Learning to diagnose cirrhosis via combined liver capsule and parenchyma ultrasound image features. In: IEEE International Conference on Bioinformatics and Biomedicine (BIBM), pp. 799–804. IEEE (2016)
23. Wu, C.C., Lee, W.L., Chen, Y.C., Lai, C.H., Hsieh, K.S.: Ultrasonic liver tissue characterization by feature fusion. Expert Syst. Appl. **39**(10), 9389–9397 (2012)
24. Wu, C.M., Chen, Y.C., Hsieh, K.S.: Texture features for classification of ultrasonic liver images. IEEE Trans. Med. Imaging **11**(2), 141–152 (1992)
25. Xu, C., Prince, J.L.: Snakes, shapes, and gradient vector flow. IEEE Trans. Image Process. **7**(3), 359–369 (1998)
26. Yamaguchi, T., Hachiya, H., Kamiyama, N., Moriyasu, F.: Examination of the spatial correlation of statistics information in the ultrasonic echo from diseased liver. Jpn. J. Appl. Phys. **41**(5S), 3585 (2002)

Jingwen Zhao received her B.E. degree from East China University of Science and Technology in 2013. She is now pursuing her Ph.D. degree in School of Computer Science, Fudan University. Her current research interests include biological image processing, medical image analysis and pattern recognition.

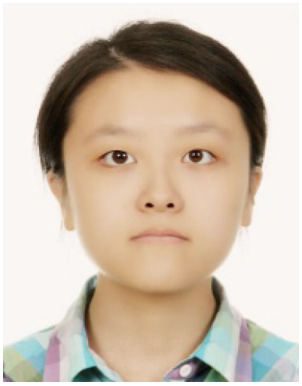

Shuo Hong Wang received her B.E. degree from East China University of Science and Technology in 2012. She is now pursuing her Ph.D. degree in School of Computer Science, Fudan University. Her research interests include multiple object tracking, biological and medical image analysis.

Xiang Liu received his M.E. degree from Jiangsu University in 1999 and BSc degree from Nanjing Normal University in 1994. He is now pursuing his Ph.D. degree in School of Computer Science, Fudan University. His current research interests include medical image analysis, biological image processing and pattern recognition. Xiang Liu is currently the associate professor and director of Computer Department with School of Electronic and Electrical Engineering of Shanghai University of Science Engineering, Shanghai, China.

Ye Liu received his Ph.D. degree in computer science in 2013 from Fudan University, Shanghai, China, and his BS degree from the Department of Computer Science and Technology at Tongji University, Shanghai, China, in 2007. He is now a faculty member with School of Automation, Nanjing University of Posts and Telecommunications. His current research interests include 3D computer vision and pattern recognition, with a special attention to 3D object detection and tracking.

Yan Qiu Chen received his Ph.D. degree from Southampton University, UK, in 1995, and his M.E. and B.E. degrees from Tongji University, Shanghai, China, in 1988 and 1985, respectively. Dr. Chen is currently a full professor and director of Computer Vision Lab with School of Computer Science of Fudan University, Shanghai, China. He had been Chairman of Department of Communication Science and Engineering from 2004 through 2007 and Associate Chairman of Department of Computer Science and Engineering from 2002 through 2004. Dr. Chen was an assistant professor with School of Electrical and Electronic Engineering of Nanyang Technological University, Singapore, from 1996 through 2001 and was a postdoctoral research fellow with Glamorgan University, UK, in 1995.